International Journal of Multiphase Flow 126 (2020) 103239

Contents lists available at ScienceDirect

International Journal of Multiphase Flow

journal homepage: www.elsevier.com/locate/ijmulflow

Shear-induced particle migration of semi-dilute and concentrated Brownian suspensions in both Poiseuille and circular Couette flow

Changwoo Kang, Parisa Mirbod*

Department of Mechanical and Industrial Engineering, University of Illinois at Chicago, 842W. Taylor Street, Chicago, IL 60607, United States

ARTICLE INFO

Article history:
Received 4 November 2019
Revised 10 January 2020
Accepted 3 February 2020
Available online 7 February 2020

Keywords:
Colloidal and Brownian suspensions
Shear-thinning effects
Particle migration
Poiseuille flow
Circular Couette flow

ABSTRACT

Neutrally buoyant colloids with small Reynolds numbers pose interesting challenges particularly when they undergo shear thinning and Brownian diffusion. Two basic flows including Poiseuille and Couette flows accompanying shear-induced particle migration are investigated in this study using direct numerical simulations (DNSs). A scaled viscosity model of colloidal suspensions considering both the shear rate and bulk particle volume fraction is employed to describe the shear-thinning behavior of suspensions. The constitutive diffusion equation proposed by Phillips et al. [*Phys. Fluids A* **4**, 30–40 (1992)] is used to model the dynamics of suspension flow. We vary the Péclet number *Pe*, from 10^{-2} to 10^{3} for the semi-dilute and dense suspensions with the bulk particle volume fraction ϕ_b, ranging from 10% to 50%. It was found that, in the limit of vanishing inertia, the distribution of volume fraction gradually flattens by increasing Brownian force. In a Poiseuille flow, the velocity of suspensions decays as the Brownian motion becomes stronger, leading to the flow rate reduction. For a circular Couette flow, the Brownian diffusion enhances the velocity of suspensions and increases the friction coefficient at the inner cylinder wall. Our study reveals that the Brownian motion is more critical for higher volume fraction values.

1. Introduction

The flow of particles suspended in a fluid is relevant to a variety of engineering and scientific applications such as transport of sediments [Snider, O'Rourke and Andrews, 1998], delivery of biochemical materials (DNA molecules and drugs) [Fan et al., 2003; Tripathi and Bèg, 2014], food processing [Lareo, Fryer and Barigou, 1997], and composite materials processing [Tucker, 1991; Petrie, 1999; Nordlund, Fernberg and Lundström, 2007]. In particular, a shear-induced particle migration occurring in either pressure or shear driven flows such as channel, pipe, and Couette flows has been a crucial issue because it can affect the flow field leading to a change of velocity profile of suspensions or induce clogging in the system [Lyon and Leal, 1998; Miller and Morris, 2006]. The focus of this work is on the suspensions of very small particles which undergo observable Brownian motion resulting from the collision of particles. In colloidal and Brownian suspensions, thermally driven stresses on the particles causing by Brownian motion can significantly impact the migration induced by the shear-driven stresses [Frank et al., 2003; Semwogerere, Morris and Weeks, 2007].

Suspensions have complex rheological behavior, which depends on the solvent properties, the spatial distribution of particles, and the microstructure [Brady and Morris, 1997]. The viscosity η of suspensions of rigid, spherical particles varies with the particle radius a, the solvent viscosity η_o, the shear rate $\dot{\gamma}$, the thermal energy kT, and the number density n [Krieger, 1963, 1972]. For neutrally buoyant suspensions, the relative viscosity $\eta_r = \eta/\eta_o$ depends on the volume fraction $\phi = 4\pi a^3 n/3$, the dimensionless shear rate (i.e., the Péclet number $\mathrm{Pe} = 6\pi\eta_o a^3\dot{\gamma}/\mathrm{kT}$), and the particle Reynolds number $\mathrm{Re} = \rho_o a^2\dot{\gamma}/\eta_o$ where ρ_o is the solvent density [Krieger, 1963, 1972; Stickel and Powell, 2005]. In the absence of inertia (i.e., at very low Reynolds numbers), the relative viscosity η_r depends only on the particle volume fraction and the shear rate as $\eta_r = f(\phi, \mathrm{Pe})$. In addition, for non-colloidal suspensions, if the Péclet number is very large ($Pe = \infty$), the relative viscosity can then be expressed as a function of the volume fraction $\eta_r = f(\phi)$ [Stickel and Powell, 2005; Hinch, 2011]. On the other hand, in the case of colloidal suspensions, *Pe* remains important and the suspensions show non-Newtonian rheological behaviors including yield stresses at high concentrations, or they present nonlinear effects such as shear rate sensitive viscosity (i.e., shear-thinning, and/or shear-thickening behavior) [Stickel and Powell, 2005; Sato, 1995; Foss and Brady, 2000; Mari et al., 2015; Marenne et al., 2017]. A dimensional analysis reported in [Krieger, 1963, 1972] has revealed that suspensions are shear-thinning when Brownian motion is significant but shear-thickening when *Re* is dominant [Semwogerere, Morris and Weeks, 2007].

* Corresponding author.
E-mail address: pmirbod@uic.edu (P. Mirbod).

https://doi.org/10.1016/j.ijmultiphaseflow.2020.103239
0301-9322/

Yield stresses have also been observed mostly at very high concentrations ($\phi > 0.5$) [Stickel and Powell, 2005; Heymann, Peukert and Aksel, 2002].

Based on the dimensional analysis reported in [Stickel and Powell, 2005], several models have been developed for the viscosity of suspensions to consider the non-Newtonian behavior of the flow. It was also reported that colloidal suspensions are shear-thinning in the range of $10^{-2} \leq Pe \leq 10^{3}$; thus, the local shear rate is strongly related to the viscosity of suspensions [Stickel and Powell, 2005]. Einstein (1906) in his pioneering work showed that in the limit of vanishing inertia and for dilute suspensions (i.e., $\phi \rightarrow 0$), the suspension viscosity is a linear function of particle volume fraction $\eta_r = 1 + 2.5\phi$. Batchelor (1977) extended Einstein's first-order equation to a second-order equation for Brownian suspensions as $\eta_r = 1 + 2.5\phi + 6.2\phi^2$. For higher volume fractions, however, the viscosity starts to increase faster than a second order polynomial [Stickel and Powell, 2005]. Cross (1965, 1970) introduced a relationship between the suspension viscosity and the shear rate for colloidal suspensions of hard spheres revealing the shear-thinning behavior as

$$\eta_r = \eta_\infty + \frac{\eta_0 - \eta_\infty}{1 + \alpha\dot{\gamma}^m} \tag{1}$$

where η_0 and η_∞ are limiting values of viscosity at zero ($\dot{\gamma} = 0$) and infinite shear rates ($\dot{\gamma} = \infty$), respectively. The constant α is a rheological fitting parameter and the exponent m depends on polydispersity of the particles [Cross, 1970].

Later on, de Kruif, et al. (1985) scaled the viscosity of colloidal suspensions as a function of both shear rate and volume fraction given by

$$\eta_r = \eta_\infty + \frac{\eta_0 - \eta_\infty}{1 + 1.31\eta_o a^3\dot{\gamma}/\mathrm{kT}} \tag{2}$$

They showed that the limiting low and high shear viscosities are only dependent on the volume fraction and can be expressed as

$$\eta_0(\dot{\gamma} \rightarrow 0) = 1 + 2.5\phi + (4 \pm 2)\phi^2 + (42 \pm 10)\phi^3 \tag{3}$$

$$\eta_\infty(\dot{\gamma} \rightarrow \infty) = 1 + 2.5\phi + (4 \pm 2)\phi^2 + (25 \pm 7)\phi^3 \tag{4}$$

They reported that these relations are valid for $\phi \sim 0.35$. The viscosities diverged at $\phi = 0.63 \pm 0.02$ for low shear limits (i.e., $\dot{\gamma} \rightarrow 0$) and at $\phi = 0.71 \pm 0.02$ for high shear limits (i.e.,$\dot{\gamma} \rightarrow \infty$), regardless of the particle size [de Kruif, et al., 1985; van der Werff and de Kruif, 1989]. For higher volume fractions, correlations of limiting viscosity were obtained by fitting experimental data to the empirical formula of Krieger and Dougherty [Krieger and Dougherty, 1959];

$$\eta_r = \left(1 - \frac{\phi}{\phi_{\max}}\right)^{-[\eta]\phi_{\max}} \tag{5}$$

Here, the suggested limiting packing fractions at which the viscosity diverges are $\phi_{\max}(\dot{\gamma} \rightarrow 0) = 0.63 \pm 0.02$ and $\phi_{\max}(\dot{\gamma} \rightarrow \infty) = 0.71 \pm 0.02$ [de Kruif, et al., 1985; van der Werff and de Kruif, 1989].

Several researchers investigated the rheology and its aspects on colloidal suspensions [Bossis and Brady, 1989; Jones, Leary and Boger, 1991; Brady, 1993; Brady and Vicic, 1995; Phung, Brady and Bossis, 1996; Yurkovetsky and Morris, 2008]; however, there have been few attempts to address the migration phenomenon of the flow of colloidal suspensions which undergoes the Brownian motion using constitutive models. In addition, while a particle migration in the flow of non-colloidal suspensions has been well-documented over the decades both experimentally and theoretically in various geometries by [Leighton and Acrivos, 1987; Fang et al., 2002; Lyon and Leal, 1998; Phillips, Armstrong and Brown, 1992; Fang et al., 2002; Miller and Morris, 2006; Ahmed and Singh, 2011, and references therein], a particle migration of the flow of Brownian suspensions in a pressure-driven flow was studied for the first time by Frank et al. (2003). The authors observed the shear-induced migration of colloidal particles flowing through rectangular channels using confocal microscopy. Concentration profiles were measured for various bulk volume fractions (ϕ_b= 0.05 ~ 0.34) and bulk Péclet numbers (Pe_B). They showed that particles move strongly toward the centerline of the channel at higher ϕ_b and Pe_B. They also developed a constitutive equation to describe the particle migration using the suspension balance model (SBM) and existing normal stress models that are functions of both ϕ_b and local Péclet number. However, they did not consider a non-Newtonian model for the viscosity of suspensions in their analysis. Semwogerere, Morris and Weeks (2007) extended the experiment of Frank et al. (2003) for varying volume fractions (ϕ_b= 0.1 ~ 0.4) and Péclet numbers (Pe_B=10 ~ 400) and investigated the influence of Brownian motion on the entrance length, which is the distance from the inlet where the concentration profile is fully developed. They found that the entrance length significantly depends on the Péclet number. For $Pe_B \ll 100$, the entrance length increases by increasing $\mathrm{Pe_B}$; however, it reaches a constant value for larger Pe_B. Moreover, the authors predicted the migration and the entrance length using the constitutive modelling proposed by Frank et al. (2003) and showed an agreement with the trends of their experiments. Thereafter, Brown et al. (2009) utilized nuclear magnetic resonance (NMR) imaging to measure the migration of particles in a capillary flow of Brownian suspension and detected the particle migration inward to the capillary center even in the dilute regime (i.e., $\phi_b <$ 0.04). Recently, colloidal suspension flows were analytically examined by Rebouças et al. (2016). They evaluated the shear-thinning effect of colloidal suspensions in a pressure-driven flow employing the viscosity model proposed by Cross (1970) (herein, reported in Eq. (1)). They showed that particles migrate differently at the centerline and near the wall which flattens the velocity profiles with a higher flow rate. However, to the best of the authors' knowledge, the impact of Brownian diffusion, coupled with the shear-thinning behavior of colloidal suspensions, on the flow and particle migration has not yet been analyzed in detail.

Herein, we study the effect of Brownian motion in the flow of neutrally buoyant and colloidal hard-sphere suspensions considering the shear-thinning behavior. A constitutive diffusion equation proposed by Phillips, Armstrong and Brown (1992) is applied to model the flow of suspensions. A viscosity model depending on both local volume fraction and shear rate is introduced to express the shear-thinning of suspension viscosity. We then couple these models with conservation equations for the flow and explore the dynamics of suspension using direct numerical simulations (DNSs). We examine the flow and migration of colloidal particles induced by the shear and Brownian motion in two basic flows including pressure-driven and circular Couette flows. Particle concentration and velocity profiles are presented for various volume fractions and Péclet numbers. The relative viscosity of suspensions determined by local concentration and shear rate is compared for different values of the Péclet number. Furthermore, volume flow rates and friction coefficients are evaluated for each flow.

The paper is organized as follows. Section II describes the mathematical equations for the flow and suspensions with the numerical procedure. The results are reported in Sec. III. The

discussion is achieved in Sec. IV and Section V addresses the conclusion.

2. Mathematical formulation

2.1. Governing equations

The flow of colloidal hard-sphere suspensions to be considered as a continuum is governed by incompressible continuity and momentum conservation equations given by

$$\nabla \cdot \mathbf{u} = \mathbf{0} \tag{6}$$

$$\rho\left(\frac{\partial \mathbf{u}}{\partial t} + \nabla \cdot (\mathbf{uu})\right) = -\nabla p + \nabla \cdot (2\eta \mathbf{S}) \tag{7}$$

Here, $\mathbf{u}$, p, and ρ are the velocity vector, pressure and density of the fluid, respectively. $\mathbf{S} = \frac{1}{2}(\nabla \mathbf{u} + \nabla \mathbf{u}^{\mathrm{T}})$ is the strain rate tensor, and η is the viscosity of the suspension.

2.2. Conservation equation for suspensions

To describe the behavior of suspension flows, we employ the constitutive model, namely the diffusive flux model (DFM) reported in [Phillips, Armstrong and Brown, 1992]. This is due to the simplicity, low computational cost, and accuracy of DFM, which is based on the prior work of Leighton and Acrivos (1987). A conservation equation for suspensions can be stated in a Lagrangian frame as

$$\frac{\partial \phi}{\partial t} + \mathbf{u} \cdot \nabla \phi = -\nabla \cdot \left(\mathbf{N}_c + \mathbf{N}_\eta + \mathbf{N}_b\right) \tag{8}$$

Here, ϕ is the particle volume fraction, $\mathbf{N}_c$, and $\mathbf{N}_\eta$ are the particle fluxes caused by spatial variation in the collision frequency and suspension viscosity, respectively. The particle fluxes can be expressed as [Phillips, Armstrong and Brown, 1992]

$$\mathbf{N}_c = -K_c a^2 \phi \nabla (\dot{\gamma}\, \phi) \tag{9}$$

$$\mathbf{N}_\eta = -K_\eta a^2 \dot{\gamma} \phi^2 \nabla (\ln \eta) \tag{10}$$

where a is the particle radius and $\dot{\gamma}$ $(= \sqrt{2\mathbf{S}..\mathbf{S}})$ is the local shear rate. The diffusion coefficients K_c and K_η are empirical constants determined by experiments.

The last term $\mathbf{N}_b$ in Eq. (8) accounts for the Brownian diffusion of suspensions and is defined as $\mathbf{N}_b = -\mathrm{Ds}\nabla\phi$. Here, D_s is the relative concentration-dependent diffusion coefficient of suspensions represented by a generalized Stokes-Einstein relation for finite volume fractions (ϕ) defined as $\mathrm{Ds}(\phi) = k_B T_s(\phi)/6\pi a \eta_s(\phi)$ [Mendoza, Santamaría-Holek and Pérez-Madrid, 2015]. Here, k_B is the Boltzmann's constant, T_s is the effective temperature, and η_s is the viscosity coefficient of suspensions. This relationship has been examined experimentally and numerically ranging from dilute to highly concentrated colloidal suspensions [van Megen, et al., 1998; Bonn, 2003; Jabbari-Farouji et al., 2007] and has shown a good fit with experimental and numerical data [Mendoza, Santamaría-Holek and Pérez-Madrid, 2015]. It should be noted that the classical Stokes-Einstein relation, $\mathrm{Do} = k_B T_o/6\pi a \eta_o$, has been deduced in for dilute suspensions.

The DFM can encounter a difficulty at points where the local shear rate ($\dot{\gamma}$) becomes zero such as the centerline of channel or pipe flow [Fang et al., 2002]. The particle volume fraction tends to approach to the maximum value ($\phi_{\max}$), causing a cusp in the profile [Lyon and Leal, 1998; Phillips, Armstrong and Brown, 1992; Fang et al., 2002]. To resolve this issue, a nonlocal stress correction has been employed by [Miller and Morris, 2006; Ahmed and Singh, 2011] to model the nonlocal suspension stresses. Herein, we apply the nonlocal stress model proposed by Miller and Morris (2006) for Poiseuille flow where a small constant nonlocal contribution depending on the particle size, the so-called $\dot{\gamma}_{\mathrm{NL}} = a_s(\varepsilon)\dot{\gamma}_s$ is counted to the local shear rate. $a_s(\varepsilon) = \varepsilon$ has been chosen by the examination, where $\varepsilon = a/h$ and h is half of the height of a channel. $\dot{\gamma}_s = U_{\max}/h$ has been used for a channel flow, where $U_{\max}$ is the centerline velocity for Poiseuille flow [Ahmed and Singh, 2011]. Thus, the particle fluxes $\mathbf{N}_c$ and $\mathbf{N}_\eta$ can be modified as [Miller and Morris, 2006; Ahmed and Singh, 2011]

$$\mathbf{N}_c = -K_c a^2 \phi \nabla [(\dot{\gamma} + \dot{\gamma}_{\mathrm{NL}})\phi] \tag{11}$$

$$\mathbf{N}_\eta = -K_\eta a^2 (\dot{\gamma} + \dot{\gamma}_{\mathrm{NL}}) \phi^2 \nabla (\ln \eta) \tag{12}$$

Note that in the present study we used the nonlocal stress model for particle fluxes only for Poiseuille flow.

2.3. Viscosity of suspensions

In this study, we consider the model proposed by de Kruif et al. (1985) (i.e., Eq. (2)) for the viscosity of colloidal suspensions with limiting viscosities determined by fitting data as [de Kruif et al., 1985]

$$\eta_0 = \left(1 - \frac{\phi}{\phi_{\max}}\right)^{-1.96} \quad \text{where } \phi_{\max} = 0.63 \tag{13}$$

$$\eta_\infty = \left(1 - \frac{\phi}{\phi_{\max}}\right)^{-1.93} \quad \text{where } \phi_{\max} = 0.71 \tag{14}$$

Accordingly, the relative viscosity η_r is locally calculated by the local concentration of suspensions $\phi(\mathbf{x}, t)$ and the local shear rate $\dot{\gamma}(\mathbf{x}, t)$ defined as $\eta = \eta(\phi, \dot{\gamma})$.

In addition, we have faced another issue arising from the viscosity model of Eq. (2) at $\dot{\gamma} \to 0$ where the relative viscosity (η_r) has a large value. In particular, for the high particle volume fraction this leads to a cusp pointed down in the profile of the particle volume fraction (ϕ) that results from the $\nabla(\ln \eta)$ term of the particle flux $\mathbf{N}_\eta$. To overcome this issue, we also introduce the nonlocal stress model proposed by Miller and Morris (2006) into the viscosity model where a small nonlocal contribution ($\dot{\gamma}_{\mathrm{NL}}$) is also added to the function of the relative viscosity given by

$$\eta_r = \eta_\infty + \frac{\eta_0 - \eta_\infty}{1 + 1.31\eta_o a^3(\dot{\gamma} + \dot{\gamma}_{\mathrm{NL}})\backslash \mathrm{kT}} \tag{15}$$

We further briefly examine the effect of this modification in the discussion section (Sec. IV).

2.4. Numerical methods

The governing equations of Eqs. (6)–(8) were discretized using a finite volume method (FVM). A second-order central difference scheme was used for spatial discretization of derivatives except for the convective term ($\mathbf{u} \cdot \nabla\phi$) of the conservation equation for suspensions (Eq. (8)), which utilized the QUICK (quadratic upstream interpolation for convective kinematics) scheme for the discretization. A hybrid scheme was applied for time advancement; nonlinear terms were explicitly advanced by a third-order Runge-Kutta scheme, and the other terms were implicitly advanced by the Crank-Nicolson method [Kang and Yang, 2011, 2012; Kang et al., 2017a, 2017b]. A fractional-step method was employed for time integration and the Poisson equation that resulted from the second stage of the fractional step method was solved by a fast Fourier transform (FFT) [Kim and Moin, 1985].

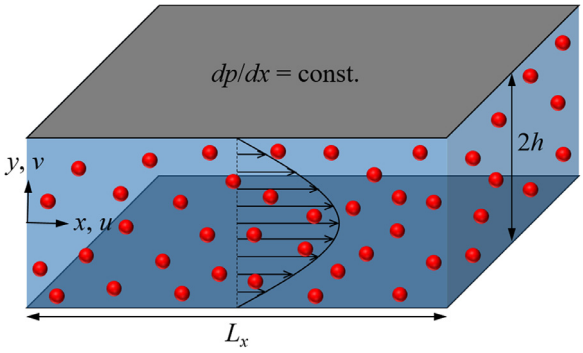

Fig. 1. Schematic diagram of suspensions in a plane Poiseuille flow driven by a constant pressure gradient (dp/dx).

3. Results

3.1. Migration in a plane Poiseuille flow

First, we consider a plane Poiseuille flow of neutrally buoyant, colloidal, and Brownian particles suspended in a viscous fluid (see Fig. 1). The flow of suspensions is driven by a constant pressure gradient (dp/dx) in a channel with the height $2h$. Direct numerical simulations were carried out on a Cartesian grid system with $64(x) \times 192(y)$ grid points and $L_x = 4h$. The grid cell was uniform in the axial direction (x), while more grid points were allocated near walls in the y-direction with $\Delta y_{\min} = 0.005h$. The no-slip condition was imposed on both walls, and the flow was assumed to be periodic in the axial direction (x).

In the DFM, the diffusion coefficients (K_c and K_η) are predicted by fitting to the experimental measurements of the particle distribution. To determine the coefficients, we compared the distribution of particle volume fraction for different values of K_c/K_η with the experimental data and theoretical predictions for colloidal and Brownian suspensions using the SBM reported by Frank et al. (2003) in Fig. 2. Here, the dimensionless parameter Pe_B is given by $Pe_B = 6\pi\eta_o a^3\dot{\gamma}_b/\mathrm{kT}$, where $\dot{\gamma}_b = u_{\max}/h$ [Frank et al., 2003] and $u_{\max}$ is the maximum axial velocity of suspensions. Frank et al. (2003) assumed that the maximum velocity is related to the bulk velocity as $u_b(= 2u_{\max}/3)$ for the Poiseuille flow of pure Newtonian fluid. We then calculated $\mathrm{Pe_B}$ using the mean velocity of suspensions. Most of the studies [Phillips, Armstrong and Brown, 1992; Lyon and Leal, 1998; Fang et al., 2002; Ahmed and Singh, 2011] have chosen the coefficients corresponding to $K_c/K_\eta = 0.66$ for Poiseuille flow of non-colloidal suspensions. However, as can be seen in Fig. 2 for the flow of colloidal suspensions considered here, the prediction of $K_c/K_\eta = 0.3$ shows the best fit with the experimental measurements. The discrepancy with the profile predicted by the SBM [Frank et al., 2003] near the center of the channel ($y = 0$) may in part be due to the application of the non-local stress model ($\dot{\gamma}_{\mathrm{NL}}$) and the viscosity model, which Frank et al. (2003) did not consider in their normal stress and viscosity models. It should be noted that comparing the concentration profiles with the data presented by Frank et al. (2003) might not be sufficient to validate our model and to choose $K_c/K_\eta = 0.3$. This is because the empirical coefficients for various flux contributions in the DFM and also the very micron size particles might affect the collective diffusion coefficient. Nevertheless, we choose the determined coefficients corresponding to $K_c/K_\eta = 0.3$ because of the lack of available data in the literatures. These need to be addressed accurately to get the best fit with the experiment.

We quantify the Brownian force with the dimensionless Péclet number $\mathrm{Pe} = \dot{\gamma}a^2/D_s$. The effective diffusion coefficient D_s depends on the particle volume fraction as proposed by the generalized Stokes-Einstein relation [Mendoza, Santamaría-Holek and Pérez-Madrid, 2015]. Herein, as a first step and simplicity of the problem we assume that the coefficient is dependent on the bulk particle volume fraction (ϕ_b), $D_s = D_o\, f(\phi_b)$, satisfying $D_s(\phi_b)\,\eta_s(\phi_b)/T_s(\phi_b) = D_o\eta_o/T_o$ given by the generalized Stokes-Einstein relation. Finally, D_s is uniform in the suspensions flow. This allows an equivalent Brownian diffusion for the same value of Pe in different bulk volume fractions (ϕ_b). The velocity $U_o = -(\mathrm{dp/dx})h^2/3\eta_o$, which indicates the mean velocity for Poiseuille flow of pure Newtonian fluid, is introduced to the definition of Pe for simplicity. Thus, the shear rate is defined as $\dot{\gamma} = U_{\max}/h$ where $U_{\max} = 3U_o/2$. U_o is also used as the velocity scale and the Péclet number is varied in the rage of $10^{-2} \le Pe \le 10^3$, which is in the typical regime of the shear-thinning to study the effect of Brownian motion as shown in the dimensional analysis reported by [Krieger, 1963, 1972; Semwogerere, Morris and Weeks, 2007]. The particle radius ratio of $\epsilon = 1/25$ is also used by referring the experiments of Frank et al. (2003).

Fig. 3(a) and (b) show distributions of particle volume fraction at varying Pe. When Brownian diffusion is weak (i.e., at high Pe), particles migrate toward the center of the channel ($y/h = 0$) which is the particle behavior of non-colloidal and non-Brownian suspensions ($Pe = \infty$). For $Pe \ge 10^2$, Brownian motion indeed does not cause a distinct impact on the concentration field. The profiles change very little and the flow of suspensions reaches the non-colloidal regime ($Pe = \infty$) where the Brownian effect becomes negligible. This is consistent with the trend of experimental observations as reported in [Frank et al., 2003; Semwogerere, Morris and Weeks, 2007; Brown et al., 2009]. In contrast, the particle migration toward the centerline weakens progressively as Brownian motion becomes stronger (i.e., as Pe decreases). This leads to the flatten distribution of local volume fraction at very small Pe ($=10^{-2}$).

The streamwise velocity profiles are plotted for various Pe in Fig. 3(c) and (d). It exhibits that the stronger Brownian diffusion (i.e., decreasing Pe) diminishes the streamwise velocity (u). The slope of velocity (du/dy) representing the local shear rate also decreases by growing Brownian diffusion. These are associated with the local volume fraction. As can be seen in Fig. 3(a) and (b), the Brownian force inhibits the migration of particles induced by the shear toward the centerline of the channel where the local shear rate is the minimum. This causes higher local volume fraction (ϕ) near channel walls ($y/h = \pm 1$) for smaller Pe which also increases the local effective viscosity. As a result, the higher viscosity leads to the large viscous friction near the walls and it reduces the axial momentum.

Local values of the relative viscosity (η_{rl}) calculated by Eq. (15) are presented for various Pe in Fig. 4. It reveals noticeable features between two regimes of Pe. As mentioned earlier, for low Pe ($Pe \le 10^1$), the local viscosity near the walls ($y/h = \pm 1$) increases with diminishing Pe. At higher ϕ_b, it is more sensitive to the Brownian motion, but the viscosity near the centerline grows as Pe increases. These are highly related to variation of the local particle volume fraction. The distributions of η_{rl} are consistent with those of the volume fraction presented in Fig. 3(b). When Pe is high (i.e., $Pe \ge 10$), by increasing Pe, the relative viscosity decreases and gradually reaches that of the flow of non-Brownian suspensions ($Pe = \infty$). However, it shows sharper cusps in the centerline ($y/h = 0$) even for very high Pe or weak Brownian force ($Pe = 10^3$) in which the profiles of particle volume fraction and axial velocity are parallel to those of non-Brownian suspensions ($Pe = \infty$). This arises from the local shear rate which becomes very small near the centerline, since the relative viscosity is determined by the local shear rate as given in Eq. (15).

In Fig. 3(c) and (d), results confirm that the velocity is diminished with increasing Brownian motion. To quantify this, we have

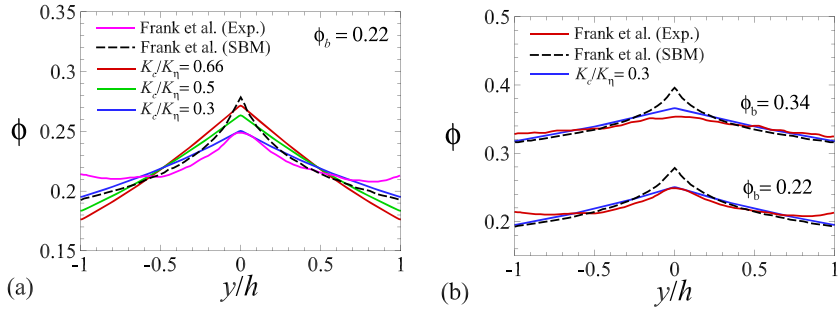

Fig. 2. Profiles of particle volume fraction (ϕ) in a Poiseuille flow for ϵ =1/25 at $Pe_B \approx 70$; (a) for different values of K_c/K_η, (b) for ϕ_b= 0.22 and ϕ_b= 0.34 with $K_c/K_\eta = 0.3$.

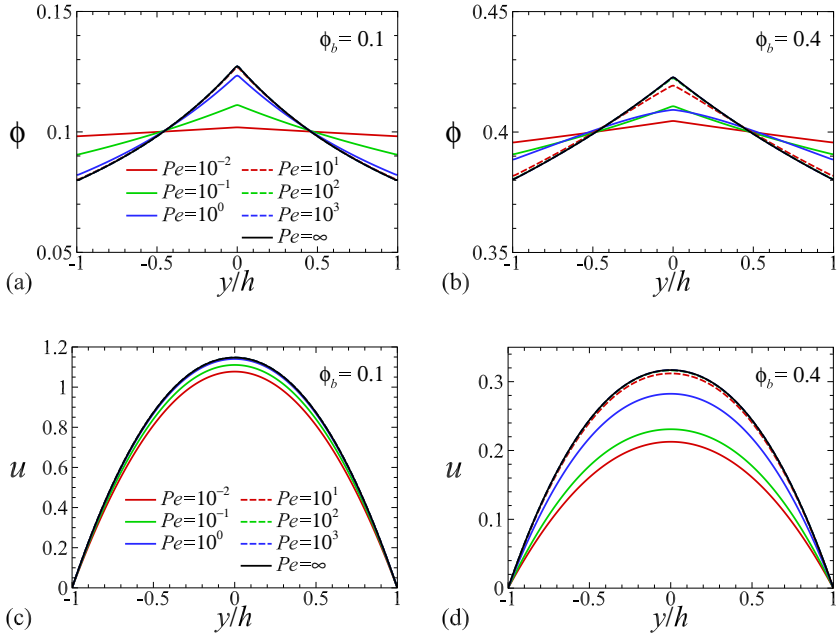

Fig. 3. (a, b) Distributions of particle volume fraction (ϕ), (c, d) profiles of the azimuthal velocity (u_θ) normalized by U_o for various Pe at ϕ_b= 0.1 and ϕ_b= 0.4.

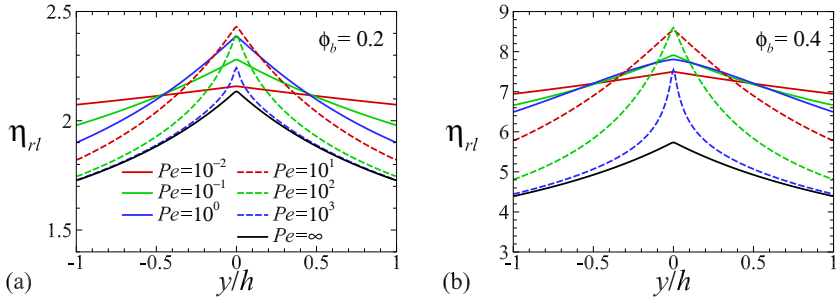

Fig. 4. Local relative viscosity (η_{rl}) for various Pe; (a) ϕ_b= 0.2, (b) ϕ_b= 0.4.

evaluated the volume flow rate (Q) of suspending fluid. The computed values of $Q = \int u\, dy$ per unit depth normal to the plane of the flow are reported in Fig. 5(a). Here, volume flow rates were normalized by that of the pure Newtonian fluid flow (i.e., $Q_o = -8h^3(dp/dx)/12\eta_o$) and dashed lines represent the values of non-Brownian suspensions for each ϕ_b. As expected, the flow rate decreases with the increase of both the Brownian diffusion (Pe^{-1}) and the bulk volume fraction (ϕ_b) showing good agreement with the velocity profiles plotted in Fig. 3(c) and (d). The effect of Brownian motion on the flow rate is more critical in dense suspension flows. For higher ϕ_b, the flow rate decays rapidly with the decrease of Pe as revealed in Fig. 5(b).

3.2. Migration of Brownian suspensions in a circular Couette flow

We then consider the flow of neutrally buoyant, colloidal, and Brownian suspensions in a circular Couette flow. As depicted in Fig. 6(a), rigid, spherical particles are suspended in a viscous fluid contained between two cylinders in which the inner cylinder of the radius R_i rotates at a constant angular velocity (Ω) and the outer one with the radius R_o is stationary. We performed DNS discretized on a cylindrical coordinate system with $96(r) \times 64(\theta)$ (Fig. 6(b)). More grid points were clustered near the wall of cylinders in the radial direction (r) with $\Delta r_{\min} = 0.005\, d$, where d

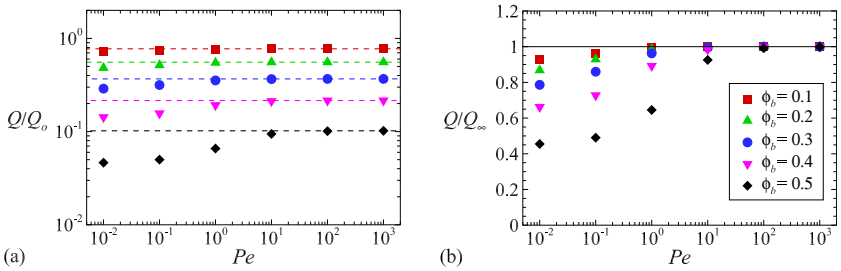

Fig. 5. Normalized volume flow rates (Q) for various values of ϕ_b and Pe; (a) Q/Q_o, (b) Q/Q_∞. Q_o is the volume flow rate for pure fluid flow, and $Q_\infty = Q(\mathrm{Pe} = \infty)$ is the value for non-Brownian and non-colloidal suspensions ($Pe = \infty$) indicated by dashed lines for each ϕ_b.

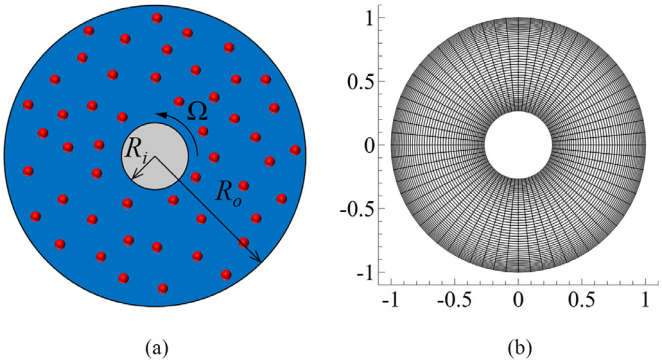

Fig. 6. (a) Schematic diagram of suspensions in a circular Couette flow with a wide gap. (b) Grid system (every other grid point is plotted in the radial direction for clarity).

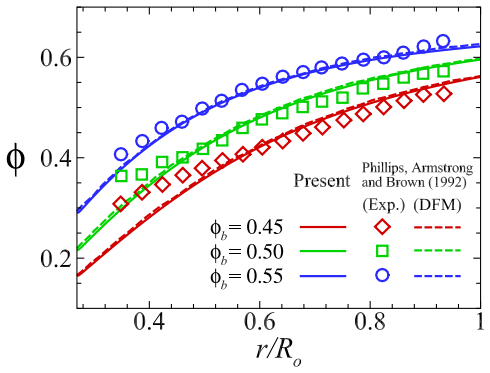

Fig. 7. Particle volume fraction (ϕ) in a circular Couette flow of non-colloidal and non-Brownian suspensions (i.e., $Pe = \infty$) for ϵ ($= a/R_o$) = 0.02836. Dashed lines, circles, squares, and triangles correspond to DFM predictions and experiments using Philips, Armstrong and Brown (1992), respectively.

($= R_o - R_i$) is the gap between two cylinders. However, the grid has a uniform size in the azimuthal direction (θ).

While numerous experiments and theoretical predictions have been carried out for non-Brownian suspensions in both concentric and eccentric cylindrical Couette cells [Leighton and Acrivos, 1987; Phillips, Armstrong and Brown, 1992; Tetlow et al., 1998; Subia et al., 1998; Fang et al., 2002; Dbouk et al., 2013; Mirbod, 2016; Sarabian et al., 2019], to the best of our knowledge the characterization of colloidal and Brownian suspensions in the circular Couette flow have not been attempted before. To validate our code, we considered the flow of non-colloidal suspensions ($Pe = \infty$). We revisited the work by Phillips, Armstrong and Brown (1992) for comparison. We performed the computations for concentrated suspensions of a particle size $\epsilon = 0.02836$ ($= a/R_o$) contained between two coaxial cylinders of the radius ratio $R_i/R_o = 0.2689$. The parameter $K_c/K_\eta = 0.66$ was also used for the diffusion coefficients of the constitutive equation [Phillips, Armstrong and Brown, 1992]. Fig. 7 shows the particle concentration profiles for several ϕ_b in comparison with those of measurements and predictions reported in Phillips, Armstrong and Brown (1992). As can be seen, particles migrate toward the outer cylinder by the shear stress arising from rotation of the inner cylinder. Our predicted profiles are in good agreement with their data. In particular, the profiles are in line with their numerical values computed by the DFM.

The dimensionless Péclet number $\mathrm{Pe} = \dot{\gamma} a^2/D_s$ that represents the quantified Brownian diffusion is defined using the mean shear rate of the Couette flow as $\dot{\gamma} = R_i\Omega/d$. This shows that Pe is determined by the effective diffusivity of the suspensions D_s, and it leads to an equivalent Brownian diffusion for a constant Pe and different ϕ_b. We adopt the geometrical and numerical parameters used for the validation in the present study (i.e., $R_i/R_o = 0.2689$, $\epsilon = 0.02836$, and $K_c/K_\eta = 0.66$). To evaluate the impact of Brownian motion, in all our computations we vary the Péclet number from 10^{-2} to 10^3.

Fig. 8(a) and (b) display profiles of particle volume fraction (ϕ) for varying Pe at $\phi_b = 0.1$ and $\phi_b = 0.4$. It turns out to be the critical role of Brownian motion is on the particle distribution. At high Pe, particles travel toward the outer cylinder wall similar to the non-colloidal particles. However, as the Brownian diffusion becomes stronger (i.e. as Pe diminishes), the local volume fraction increases near the inner wall and decreases near the outer wall. Finally, at the lowest Pe, the profile of ϕ flattens out with the strong Brownian motion. Therefore, it could be concluded that the Brownian diffusion limits the shear-induced particle migration toward the region of the low shear rate and particles will be distributed evenly within the gap of the Couette cell.

The azimuthal velocity (u_θ) profiles varying Pe for $\phi_b = 0.1$ and $\phi_b = 0.4$ are presented in Fig. 8(c) and (d). As can be seen, Brownian motion also alters the velocity distribution between two cylinders. The velocity is amplified by increasing Brownian diffusion (i.e., decrease of Pe). Hence, the slope of velocity profiles near the inner cylinder ($|\partial u_\theta/\partial r|$ at $r = R_i$) decays as Pe decreases. The impact of Brownian motion is more significant at higher ϕ_b. It could be interpreted as the migrated particle volume fraction. As illustrated in Fig. 8, the local particle volume fraction near the inner cylinder is higher for lower Pe. This causes a larger suspension viscosity, then a stronger viscous drag force acts on the fluid. As a result, the drag force enhances the velocity of the flow driven by the shear. Meanwhile, the velocity rises more sharply at highly dense suspensions.

The local relative viscosities (η_{rl}) given by Eq. (15) at different Pe for $\phi_b = 0.2$ and $\phi_b = 0.4$ are plotted in Fig. 9. The values are well correlated with the distribution of particle volume fraction provided in Fig. 8(a) and (b). In the vicinity of the inner cylinder, the high concentration induced by the strong Brownian motion re-

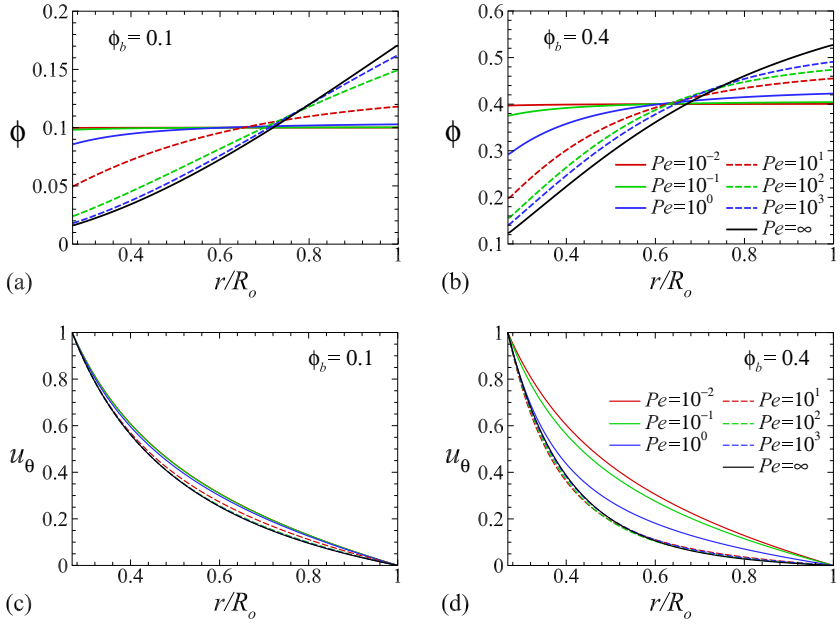

Fig. 8. (a, b) Distributions of particle volume fraction (ϕ), (c, d) profiles of the azimuthal velocity (u_θ) normalized by $R_i\Omega$ for various Pe at ϕ_b= 0.1 and ϕ_b= 0.4.

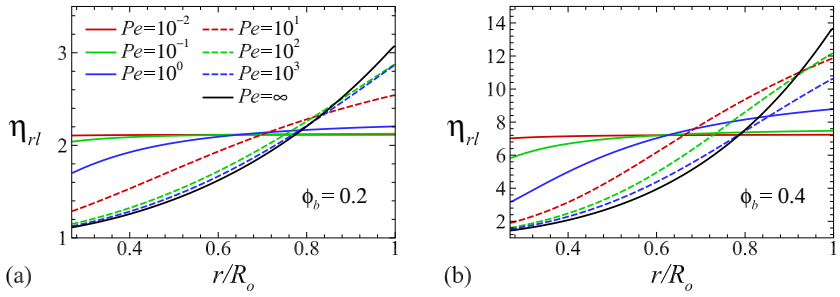

Fig. 9. Profiles of the local relative viscosity (η_{rl}) for various Pe; (a) ϕ_b= 0.2, (b) ϕ_b= 0.4.

sults in a large value of suspension relative viscosity. It creates intense viscous drag force in the fluid and larger velocity of the flow as stated above. The relative viscosity diminishes near the inner cylinder as the local particle volume fraction decreases with the weakening of the Brownian diffusion (i.e., increasing of Pe). On the other hand, η_{rl} is rather complicated close to the outer cylinder. It appears that the function of η_{rl} (Eq. (15)) is very sensitive to high volume fraction and low shear rate. When Brownian motion impact is low (high Pe), particles migrate toward the outer cylinder leading to higher concentration of particles in the outer region of cylinder. Accordingly, this causes the complex behavior of the viscosity depending on the particle volume fraction and local shear rate; thus, the value of η_{rl} is independent of Pe in the vicinity of the outer wall.

The friction coefficient C_M, which is a dimensionless measure of the torque acting on the inner cylinder, has been evaluated to identify the influence of Brownian motion on the momentum transfer. For this study, it can be given by [Kang, Yang and Mutabazi, 2015; Guillerm et al., 2015]

$$C_M = \frac{M}{\rho\pi\Omega^2 R_i^4/2} \tag{16}$$

where M is the momentum over the cylindrical surface [Kang, Yang and Mutabazi, 2015; Guillerm et al., 2015]. The variation of C_M against Pe for all values of ϕ_b is illustrated in Fig. 10. The coefficients were normalized by the friction coefficient for pure fluid flow $C_{M_o} = -\frac{1}{e(1+e)}\frac{8\eta_o}{\rho_o R_i\Omega d}$ where $e = R_i/R_o$ in Fig. 10(a) [Kang, Yang

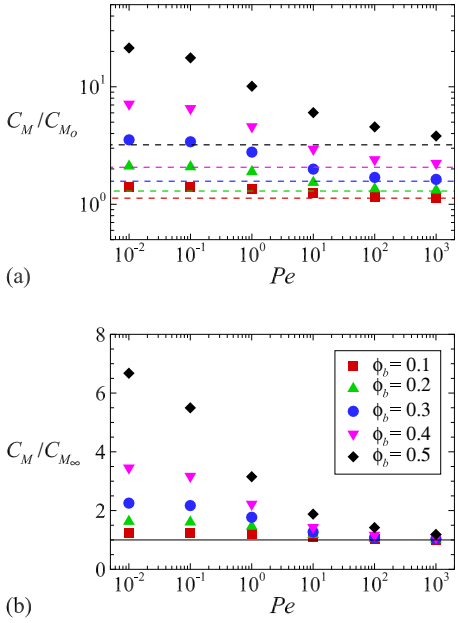

Fig. 10. Normalized friction coefficients (C_M) for different values of ϕ_b and Pe; (a) C_M/C_{M_o}, (b) C_M/C_{M_∞}. C_{M_o} is the friction coefficient for pure fluid flow, and C_{M_∞} is the value for non-Brownian suspensions ($Pe = \infty$) indicated by dashed lines for each ϕ_b.

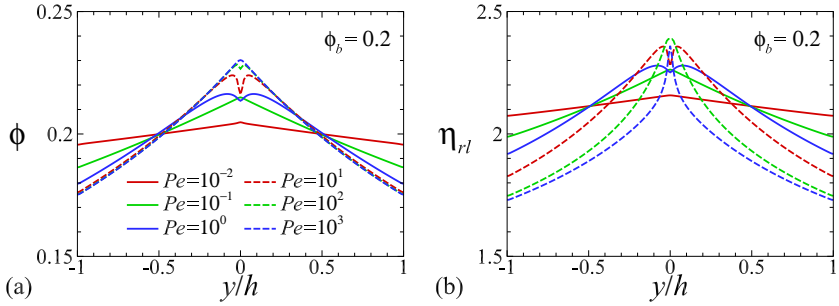

Fig. 11. (a) Concentration profiles (ϕ) and (b) profiles of the local relative viscosity (η_{rl}) in the plane Poiseuille flow without the non-local contribution ($\dot{\gamma}_{\mathrm{NL}}$) in Eq. (15) for ϕ_b= 0.2.

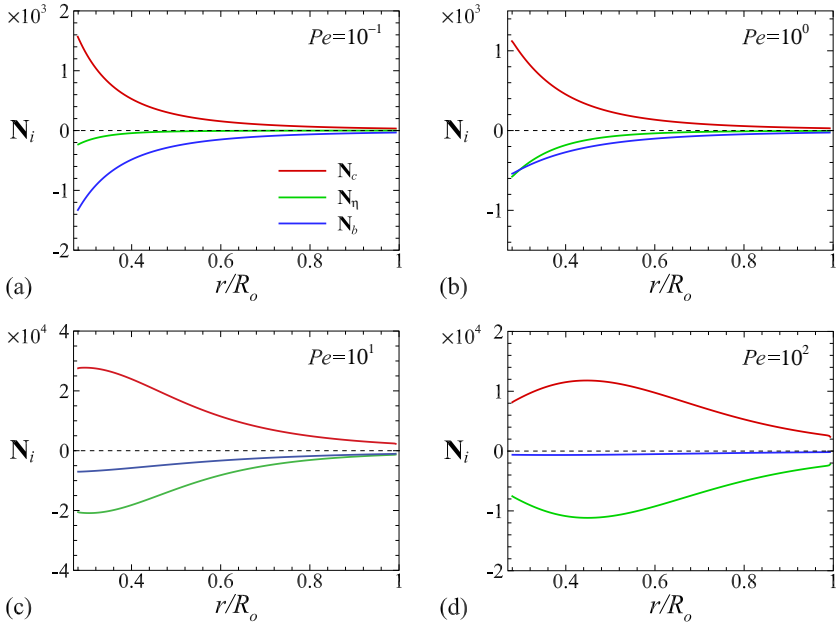

Fig. 12. Comparison of particle fluxes ($\mathbf{N}_i$) normalized by $R_i\Omega$ for various Pe and ϕ_b= 0.3 in a circular Couette flow; (a) $Pe = 10^{-1}$, (b) $Pe = 10$, (c) $Pe = 10^1$, (d) $Pe = 10^2$.

and Mutabazi, 2015; Guillerm et al., 2015]. The dashed lines represent the values for non-Brownian suspensions ($C_{M_\infty} = C_M(\mathrm{Pe} = \infty)$) at each ϕ_b. It can be observed that the concentrated suspensions cause larger friction coefficients, showing $C_M / C_{M_o} > 1$. As a matter of fact, a stronger torque is exerted on the inner cylinder by the suspending fluid. As the Brownian force becomes increasingly dominant and the suspensions become denser, C_M gradually rises. However, there is no detectable impact for the flow of dilute suspensions with very weak Brownian diffusion (i.e., very high Pe). Furthermore, as can be seen in Fig. 10(b), the effect of Pe is more critical for higher ϕ_b. The relative friction coefficient (C_M / C_{M_∞}) grows more sharply as Pe diminishes.

4. Discussion

Fully-developed flows of colloidal, Brownian, neutrally buoyant suspensions of rigid, spherical particles in both Poiseuille and circular Couette flow have been considered in this study. A viscosity model, proposed by de Kruif et al. (1985), as a function of local particle volume fraction and shear rate has been introduced to express the shear-thinning effect of colloidal and Brownian suspensions. As stated in Sec. II, we have been confronted with a difficulty when we apply the viscosity model of Eq. (2). Fig. 11 displays the distributions of particle volume fraction (ϕ) and local relative viscosity (η_{rl}) predicted with the viscosity function of Eq. (2), for various Pe at ϕ_b= 0.2 in the plane Poiseuille flow. As mentioned earlier, sharp cusps pointed down are detected for some cases at the center ($y/h = 0$). These features can also be seen in the particle concentration profiles reported by Rebouças et al. (2016) who considered the viscosity model of Cross (1970), presented in Eq. (1), for the flow of colloidal suspensions through a cylindrical tube. This is linked to the shear rate $\dot{\gamma}$, since the local shear rate approaches to zero ($\dot{\gamma} \to 0$) near the point and then it causes discontinuous cusps in the distribution of the viscosity. Finally, it results in the discontinuity of concentration profile originated from the $\nabla(\ln\eta)$ term of the particle flux $\mathbf{N}_\eta$ at the center. To improve this difficulty, we have modified the function of the viscosity model by adopting the nonlocal contribution ($\dot{\gamma}_{\mathrm{NL}}$) to the model as given in Eq. (15). The results obtained for both ϕ and η_{rl} are shown in Figs. 3 and 4.

The particle migration of colloidal particles influenced by Brownian motion has been investigated by varying the Péclet number Pe in this study. Our result has revealed that the Brownian diffusion inhabits the shear-induced particle migration. To further analyze the migration, we have compared the particle fluxes ($\mathbf{N}_i$) expressed in the conservation equation for particles in Eq. (8). Fig. 12 illustrates the variation of particle fluxes for several Pe in the circular Couette flow. The flux $\mathbf{N}_c$ arising from the varying collision frequency is balanced by the flux $\mathbf{N}_\eta$ caused by the spatial variation of the suspension viscosity (η) and the Brownian diffusive flux $\mathbf{N}_b$. As expected, at low Pe, the contribution of $\mathbf{N}_b$ to the total flux is large and it is more dominant compare to the flux $\mathbf{N}_\eta$. How-

ever, the flux $\mathbf{N}_b$ and its contribution progressively diminishes with increasing *Pe*. For high *Pe*, the Brownian flux ($\mathbf{N}_b$) becomes very small and negligible compare to other fluxes. This analysis strongly supports our findings which address the role of the Brownian diffusion on the particle migration.

5. Conclusion

This work provides the first evidence on the shear-thinning behavior and Brownian motion effects of the flow of colloidal suspensions in both Poiseuille and circular Couette flow. In summary, we have numerically examined the flow of colloidal and Brownian suspensions of rigid, spherical particles by considering the shear-thinning impact of the suspensions. The constitutive equation modeling of the dynamics of suspensions has been solved with the flow equations using direct numerical simulations. To describe the shear-thinning viscosity of suspensions, the scaled viscosity model defined as a function of both local shear rate and concentration has been used. Pressure-driven and Couette flows of colloidal and Brownian suspensions have been studied to clarify the flow phenomena and the shear-induced particle migration in these flows. We have varied the Péclet number which quantifies the Brownian diffusion to elucidate the impact of Brownian motion on the flow and the particle migration.

For Poiseuille flow, our prediction on the particle distribution shows good agreement with the available experimental data. As the Brownian motion becomes stronger (i.e., as *Pe* decreases), the particle migration caused by the shear toward to the center of the channel is restricted. The particle distribution flattens out with very large Brownian diffusion (or at very low *Pe*). The velocity of suspensions decays with the stronger Brownian motion, since the higher concentration close to the channel walls grows the local viscosity and the viscous friction on the walls. The reduction in the velocity by the Brownian diffusion effect has been quantified by evaluating the volume flow rate (Q) of suspending fluid. It has been shown that increasing both Brownian diffusion and suspensions volume fraction causes the reduction of the flow rate. This effect is more critical in dense suspension flows (i.e., at high ϕ_b).

In the circular Couette flow, Brownian motion inhibits the particle transport toward to the outer cylinder wall by intensifying the Brownian diffusive flux. The very strong Brownian motion (i.e., very low *Pe*) makes the profile of particle volume fraction flat. Furthermore, it enhances the velocity of suspensions between two cylinders. The enhancement is more distinct for highly dense suspensions (i.e., at high ϕ_b). Although the slope of the velocity decreases in the vicinity of the inner cylinder wall as *Pe* reduces, the viscosity of suspensions grows since the local particle volume fraction increases. As a result, it leads to the rise of the friction coefficient (C_M) on the inner cylinder wall. The coefficient rises by decreasing *Pe* and increasing ϕ_b.

This study would also be a framework for the future study of Brownian suspensions and shed lights on the understanding of colloidal suspensions flow in various geometries. A systematic experimental investigation of flow in a circular Couette cell is needed.

Declaration of Competing Interest

The authors declare that they have no known competing financial interests or personal relationships that could have appeared to influence the work reported in this paper.

Author Statement

Changwoo Kang: Data analysis, Writing and Original draft preparation

Parisa Mirbod: Supervision, Writing, Reviewing, and Editing

Acknowledgements

This work has been supported partially by National Science Foundation award #1854376 and partially by Army Research Office award #W911NF-18–1–0356.

Supplementary materials

Supplementary material associated with this article can be found, in the online version, at doi:10.1016/j.ijmultiphaseflow.2020.103239.

References

Ahmed, G.M.Y., Singh, A., 2011. Numerical simulation of particle migration in asymmetric bifurcation channel. J. Non-Newton. Fluid 166, 42–51. doi:10.1016/j.jnnfm.2010.10.004.

Batchelor, G.K., 1977. The effect of Brownian motion on the bulk stress in a suspension of spherical particles. J. Fluid Mech. 83, 97–117. doi:10.1017/S0022112077001062.

Bonn, D., 2003. Stokes-Einstein relations and the fluctuation-dissipation theorem in a supercooled colloidal fluid. J. Chem. Phys. 118, 2005–2009. doi:10.1063/1.1532349.

Bossis, G., Brady, J.F., 1989. The rheology of Brownian suspensions. J. Chem. Phys. 91, 1866–1874. doi:10.1063/1.457091.

Brady, J.F., 1993. The rheological behavior of concentrated colloidal dispersions. J. Chem. Phys. 99, 567–581. doi:10.1063/1.465782.

Brady, J.F., Vicic, M.A., 1995. Normal stresses in colloidal dispersions. J. Rheol. 39, 545–566. doi:10.1122/1.550712.

Brady, J.F., Morris, J.F., 1997. Microstructure of strongly sheared suspensions and its impact on rheology and diffusion. J. Fluid Mech. 348, 103–139. doi:10.1017/S0022112097006320.

Brown, J.R., Fridjonsson, E.O., Seymour, J.D., Codd, S.L., 2009. Nuclear magnetic resonance measurement of shear-induced particle migration in Brownian suspensions. Phys. Fluids 21, 093301. doi:10.1063/1.3230498.

Cross, M.M., 1965. Rheology of non-Newtonian fluids: a new flow equation for pseudoplastic systems. J. Colloid Sci. 20, 417–437. doi:10.1016/0095-8522(65)90022-X.

Cross, M.M., 1970. Kinetic interpretation of non-Newtonian flow. J. Colloid Interfac. Sci. 33, 30–35. doi:10.1016/0021-9797(70)90068-8.

Dbouk, T., Lemaire, E., Lobry, L., Moukalled, F., 2013. Shear-induced particle migration: predictions from experimental evaluation of the particle stress tensor. J. Non-Newton. Fluid 198, 78–95. doi:10.1016/j.jnnfm.2013.03.006.

Einstein, A., 1906. A new determination of molecular dimensions. Ann. Phys. 19, 289.

Fan, X., Phan-Thien, N., Yong, N.T., Wu, X., Xu, D., 2003. Microchannel flow of a macromolecular suspension. Phys. Fluids 15, 11–21. doi:10.1063/1.1522750.

Fang, Z., Mammoli, A.A., Brady, J.F., Ingber, M.S., Mondy, L.A., Graham, A.L., 2002. Flow-aligned tensor models for suspension flows. Int. J. Multiphase Flow 28, 137–166. doi:10.1016/S0301-9322(01)00055-6.

Foss, D.R., Brady, J.F., 2000. Structure, diffusion and rheology of Brownian suspensions by Stokesian Dynamics simulation. J. Fluid Mech. 407, 167–200. doi:10.1017/S0022112099007557.

Frank, M., Anderson, D., Weeks, E.R., Morris, J.F., 2003. Particle migration in pressure-driven flow of a Brownian suspension. J. Fluid Mech. 493, 363–378. doi:10.1017/S0022112003006001.

Guillerm, R., Kang, C., Savaro, C., Lepiller, V., Prigent, A., Yang, K.-S., Mutabazi, I., 2015. Flow regimes in a vertical Taylor-Couette system with a radial thermal gradient. Phys. Fluids 27, 094101. doi:10.1063/1.4930588.

Heymann, L., Peukert, S., Aksel, N., 2002. On the solid-liquid transition of concentrated suspensions in transient shear flow. Rheol. Acta 41, 307–315. doi:10.1007/s00397-002-0227-1.

Hinch, E.J., 2011. The measurement of suspension rheology. J. Fluid Mech. 686, 1–4. doi:10.1017/jfm.2011.350.

Jabbari-Farouji, S., Mizuno, D., Atakhorrami, M., MacKintosh, F.C., Schmidt, C.F., Eiser, E., Wegdam, G.H., Bonn, D., 2007. Fluctuation-dissipation theorem in an aging colloidal glass. Phy. Rev. Lett. 98, 108302. doi:10.1103/PhysRevLett.98.108302.

Jones, D.A.R., Leary, B., Boger, D.V., 1991. The rheology of a concentrated colloidal suspension of hard spheres. J. Colloid Interface Sci. 147, 479–495. doi:10.1016/0021-9797(91)90182-8.

Kang, C., Yang, K.S., 2011. Heat transfer characteristics of baffled channel flow. ASME J. Heat Transfer 133, 091901. doi:10.1115/1.4003829.

Kang, C., Yang, K.-S., 2012. Flow instability in baffled channel flow. Int. J. Heat Fluid Flow 38, 40–49. doi:10.1016/j.ijheatfluidflow.2012.08.002.

Kang, C., Yang, K.-S., Mutabazi, I., 2015. Thermal effect on large-aspect-ratio couette-taylor system: numerical simulations. J. Fluid Mech. 771, 57–78. doi:10.1017/jfm.2015.151.

Kang, C., Meyer, A., Mutabazi, I., Yoshikawa, H.N., 2017a. Radial buoyancy effects on momentum and heat transfer in a circular couette flow. Phys. Rev. Fluids 2, 053901. doi:10.1103/PhysRevFluids.2.053901.

Kang, C., Meyer, A., Yoshikawa, H.N., Mutabazi, I., 2017b. Numerical simulation of circular couette flow under a radial thermos-electric body force. Phys. Fluids 29, 114105. doi:10.1063/1.4994244.
Kim, J., Moin, P., 1985. Application of a fractional-step method to incompressible navier-stokes equations. J. Comp. Phys. 59, 308–323. doi:10.1016/0021-9991(85)90148-2.
Krieger, I.M., Dougherty, T.J., 1959. A mechanism for non-Newtonian flow in suspensions of rigid spheres. Trans. Soc. Rheol. 3, 137–152. doi:10.1122/1.548848.
Krieger, I.M., 1963. A dimensional approach to colloid rheology. trans. rheol.. Soc 7, 101–109. doi:10.1122/1.548947.
Krieger, I.M., 1972. Rheology of monodisperse lattices. Adv. Colloid Interface Sci. 3, 111–136. doi:10.1016/0001-8686(72)80001-0.
de Kruif, C.G., van Iersel, E.M.F., Vrij, A., Russel, W.B., 1985. Hard sphere colloidal dispersions: viscosity as a function of shear rate and volume fraction. J. Chem. Phys. 83, 4717–4725. doi:10.1063/1.448997.
Lareo, C., Fryer, P.J., Barigou, M., 1997. The fluid mechanics of two-phase solid-liquid food flows: a review. Food Bioprod. Process. 75, 73–105. doi:10.1205/096030897531405.
Leighton, D., Acrivos, A., 1987. The shear-induced migration of particles in concentrated suspensions. J. Fluid Mech. 181, 415–439. doi:10.1017/S0022112087002155.
Lyon, M.K., Leal, L.G., 1998. An experimental study of the motion of concentrated suspensions in two-dimensional channel flow. part 1. monodisperse system.. J. Fluid Mech 363, 25–56. doi:10.1017/S0022112098008817.
Marenne, S., Morris, J.F., Foss, D.R., Brady, J.F., 2017. Unsteady shear flows of colloidal hard-sphere suspensions by dynamic simulation. J. Rheol. 61, 477–501. doi:10.1122/1.4979005.
Mari, R., Seto, R., Morris, J.F., Denn, M.M., 2015. Discontinuous shear thickening in brownian suspensions by dynamic simulation. Proc. Natl. Acad. Sci. U.S.A. 112, 15326–15330. doi:10.1073/pnas.1515477112.
van Megen, W., Mortensen, T.C., Williams, S.R., Müller, J., 1998. Measurement of the self-intermediate scattering function of suspensions of hard spherical particles near the glass transition. Phys. Rev. E 58, 6073–6085. doi:10.1103/PhysRevE.58.6073.
Mendoza, C.I., Santamaría-Holek, I., Pérez-Madrid, A., 2015. Effective temperatures and the breakdown of the stokes-einstein relation for particle suspensions. J. Chem. Phys. 143, 104506. doi:10.1063/1.4930550.
Miller, R.M., Morris, J.F., 2006. Normal stress-driven migration and axial development in pressure-driven flow of concentrated suspensions. J. Non-Newton. Fluid 135, 149–165. doi:10.1016/j.jnnfm.2005.11.009.
Mirbod, P., 2016. Two-dimensional computational fluid dynamical investigation of particle migration in rotating eccentric cylinders using suspension balance model. Int. J. Multiphase Flow 80, 79–88. doi:10.1016/j.ijmultiphaseflow.2015.11.002.
Nordlund, M., Fernberg, S.P., Lundström, T.S., 2007. Particle deposition mechanisms during processing of advanced composite materials. Composites Part A 38, 2182–2193. doi:10.1016/j.compositesa.2007.06.009.
Petrie, C.J.S., 1999. The rheology of fibre suspensions. J. Non-Newton. Fluid 87, 369–402. doi:10.1016/S0377-0257(99)00069-5.
Phillips, R.J., Armstrong, R.C., Brown, R.A., 1992. A constitutive equation for concentrated suspensions that accounts for shear-induced particle migration. Phys. Fluids A 4, 30–40. doi:10.1063/1.858498.
Phung, T.N., Brady, J.F., Bossis, G., 1996. Stokesian dynamics simulation of brownian suspensions. J. Fluid Mech. 313, 181–207. doi:10.1017/S0022112096002170.
Rebouças, R.B., Siqueira, I.R., de Souza Mendes, P.R., Carvalho, M.S., 2016. On the pressure-driven flow of suspensions: particle migration in shear sensitive liquids. J. Non-Newton. Fluid 234, 178–187. doi:10.1016/j.jnnfm.2016.06.001.
Sarabian, M., Firouznia, M., Metzger, B., Hormozi, S., 2019. Fully developed and transient concentration profiles of particulate suspensions sheared in a cylindrical couette cell. J. Fluid Mech. 862, 659–671. doi:10.1017/jfm.2018.982.
Sato, T., 1995. Rheology of suspensions. J. Coat. Technol. 67, 69–79.
Semwogerere, D., Morris, J.F., Weeks, E.R., 2007. Development of particle migration in pressure-driven flow of a brownian suspension. J. Fluid Mech. 581, 437–451. doi:10.1017/S0022112007006088.
Snider, D.M., O'Rourke, P.J., Andrews, M.J., 1998. Sediment flow in inclined vessels calculated using a multiphase particle-in-cell model for dense particle flows. Int. J. Multiphase Flow 24, 1359–1382. doi:10.1016/S0301-9322(98)00030-5.
Stickel, J.J., Powell, R.L., 2005. Fluid mechanics and rheology of dense suspensions. Annu. Rev. Fluid Mech. 37, 129–149. doi:10.1146/annurev.fluid.36.050802.122132.
Subia, S.R., Ingber, M.S., Mondy, L.A., Altobelli, S.A., Graham, A.L., 1998. Modelling of concentrated suspensions using a continuum constitutive equation. J. Fluid Mech. 373, 193–219. doi:10.1017/S0022112098002651.
Tetlow, N., Graham, A.L., Ingber, M.S., Subia, S.R., Mondy, L.A., Altobelli, S.A., 1998. Particle migration in a couette apparatus: experiment and modeling. J. Rheol. 42, 307–327. doi:10.1122/1.550954.
Tripathi, D., Bèg, O.A., 2014. A study on peristaltic flow of nanofluids: application in drug delivery systems. Int. J. Heat Mass Transfer 70, 61–70. doi:10.1016/j.ijheatmasstransfer.2013.10.044.
Tucker, C.L., 1991. Flow regimes for fiber suspensions in narrow gaps. J. Non-Newton. Fluid 39, 239–268. doi:10.1016/0377-0257(91)80017-E.
van der Werff, J.C., de Kruif, C.G., 1989. Hard-sphere colloidal dispersions: the scaling of rheological properties with particle size, volume fraction, and shear rate. J. Rheol. 33, 421–454. doi:10.1122/1.550062.
Yurkovetsky, Y., Morris, J.F., 2008. Particle pressure in sheared brownian suspensions. J. Rheol. 52, 141–164. doi:10.1122/1.2807443.